

In situ multiphoton optical tomography of hair follicles in mice

Julia G. Lyubovitsky

Tatiana B. Krasieva

University of California
Beckman Laser Institute
Laser Microbeam and Medical Program
Irvine, California 92612

Xiaoman Xu

Bogi Andersen

University of California
Departments of Medicine (Endocrinology) and
Biological Chemistry
Irvine, California 92697

Bruce J. Tromberg

University of California
Beckman Laser Institute
Laser Microbeam and Medical Program
Irvine, California 92612

Abstract. We report multiphoton *in situ* optical sectioning of hair follicles in mice and a preliminary investigation of the pathological hair follicles in a transgenic mouse model. Using this imaging technology, we rapidly obtain detailed three-dimensional (3-D) reconstructions of individual hair follicles. No staining or mechanical sectioning is involved, since multiphoton microscopy coregisters two-photon excited fluorescence (TPF) from cells and second harmonic generation (SHG) signals from the extracellular matrix (ECM). These signals are ideally suited for estimating molecularly encoded hair follicular 3-D geometries, including sizes of the follicular orifices and their angles relative to the skin surface. In the normal hair follicles, spectral separation of SHG signals generated by the ECM of the hair follicle from that of intrinsic cellular fluorescence revealed intricate spatial interaction of the cellular components with the surrounding connective tissue. In the pathological hair follicles, these were clearly modified. In particular, in the transgenic mice, we observed lack of cellular fluorescence and significantly shallower angles of follicular orifices with respect to the skin surface. The combination of TPF with SHG is sensitive to structural changes in cells and extracellular matrix brought on by normal hair follicle physiology and specific gene alterations. © 2007 Society of Photo-Optical Instrumentation Engineers. [DOI: 10.1117/1.2764462]

Keywords: hair follicle; dermis; microscopy; two-photon; collagen; extracellular matrix.

Paper 06281R received Oct. 10, 2006; revised manuscript received Apr. 10, 2007; accepted for publication Apr. 10, 2007; published online Aug. 31, 2007.

1 Introduction

Biomedical imaging using multiphoton microscopy (MPM) combines backscattered second harmonic generation (SHG) and two-photon fluorescence (TPF) signals. Combined TPF and SHG has been widely employed to nondestructively obtain structural and functional information at depth in thick, living tissues with high resolution and contrast.^{1–11} A potential of this imaging modality for *in vivo* application is vast and remains largely unexplored. It ranges from minimally invasive and rapid diagnoses of pathologies to serving as a rapid add-on to many biochemical analyses.

The purpose of this report is to establish the use of MPM to image deep into hair follicles *in situ* without mechanical sectioning or application of exogenous dyes. This information will lead to establishing minimally invasive and prompt imaging modalities to characterize various features of hair follicles, including extracellular matrix (ECM) cell interactions, hair follicular sizes, angles relative to skin surface, and overall three-dimensional (3-D) geometry—all of which are dictated by a complex interplay of molecular signals reviewed in Ref. 12. Ultimately, it may aid our understanding of the fundamental mechanisms underlying normal hair follicle physiology, development of its pathologies, and will help to evalu-

ate the efficacy of administered treatments in a noninvasive manner.

The skin acts as a permeability barrier and is one of the main organs through which we interact with the external environment. Its heterogeneous structure is derived from ectoderm and mesoderm of an embryo that gives rise to epidermis and dermis, respectively. The specialized skin appendages such as sweat glands, sensory nerves, and hair follicles are also derived from ectoderm/mesoderm.

The hair follicles are self-renewing mini-organs. They are in a continuous balance between epithelial cell division and terminal differentiation. The disruption of this balance is a feature of many skin diseases and various epidermal cancers, including basal cell carcinoma. Normal hair follicle morphogenesis follows a highly conserved evolutionary strategy for organ development that involves epithelial-mesenchymal interactions dictating all stages of induction and morphogenesis. The bulge region of the hair follicle (Fig. 1) is suggested to be a niche of multipotent stem cells.¹³ Growing evidence suggests that some of these cells become activated and migrate out of the hair follicle to regenerate epidermis during wound healing.

While formation of the hair follicles occurs once in a lifetime of an individual, each follicle cycles continually through the distinct stages of growth (anagen), regression (catagen),

Address all correspondence to Julia G. Lyubovitsky, University of California, Beckman Laser Institute, 1002 Health Sciences Road East, Irvine, CA 92612; Tel: 949-824-8705; Fax: 949-824-8413; Email: jlyubovi@uci.edu

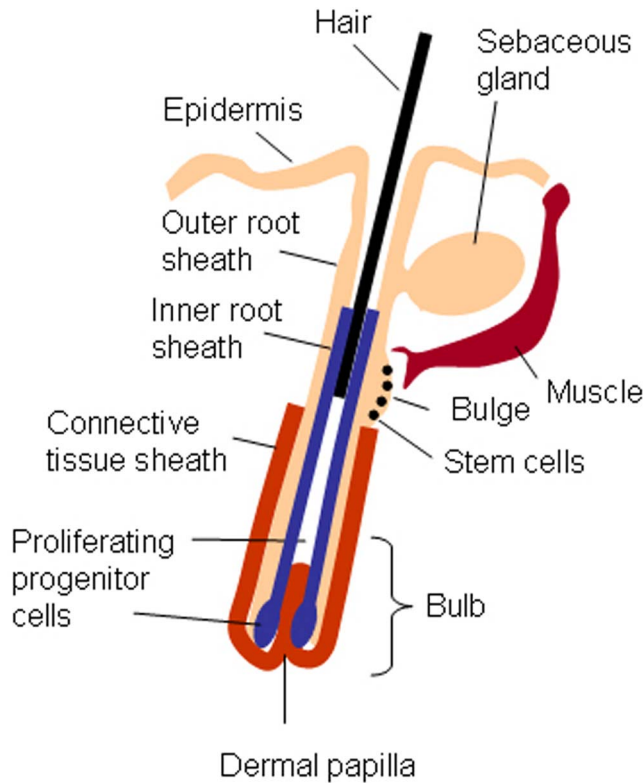


Fig. 1 A diagram of the hair follicle in the anagen phase.

rest (telogen), and shedding (exogen).¹⁴ The duration of anagen is genetically programmed and determines the shaft's maximum length. Follicle regression during the catagen phase results from controlled programmed cell death. During this stage, most of the epithelial cells in the follicle below the bulge region (Fig. 1) are destroyed, with dermal papilla remaining intact. In telogen, the resulting hair remains anchored until it is shed during exogen. Understanding mechanisms of hair follicle cycling is one of the most important questions in basic hair biology, particularly due to its great importance to the entire architecture and growth of the skin organ.¹² Here we demonstrate that 3-D multiphoton imaging offers a unique approach to aid rapidly and nondestructively in this quest.

In this work, we use endogenous cellular fluorescence and SHG signals from the ECM to image deep into normal hair follicles in mice. We show how these images can be used to determine quantitative features of hair follicular structures, which potentially can be followed as a function of hair cycle. The sizes of follicular orifices, angles of cellular components with respect to the surface of the connective tissue, and overall 3-D geometries, including rotations in the opening of ECM to accommodate cellular components, can be quantitatively estimated.

We extended the MPM *in situ* optical tomography to evaluate perturbed hair follicles in a transgenic mouse model of Clim transcriptional factors, co-activators LIM domain proteins¹⁵⁻²⁰ that displayed abnormal hair cycling. The transgenic animals were specifically created to test the role of Clim genes in the development of stratified epithelial tissues. In particular, the dominant negative (DN) Clim was expressed in stratified epithelial tissues of mice using keratin 14 (K14) pro-

motor (K14-DN-Clim mice). The DN-Clim blocks the function of normal Clim, and the K14 promoter targets the expression of the gene to stratified epithelial tissues including skin, hair, and cornea. The transgenic animals develop progressive corneal abnormalities and hair loss, and some mice develop chronic wounds on the upper parts of their back. The generation and characterization of animals is discussed in a separate paper.²¹ In these mice, we detect significantly shallower angles of the follicular orifices with respect to the skin surface compared to the normal phenotype.

Genetically altered tissues often display aberrant mechanical responses, making it difficult to rely on standard histology as a means of correlating structural pathologies with gene and protein expression profiles. In this report, we show that *in situ* endogenous cellular fluorescence and SHG signals are two nondestructive probes that are sensitive to structural changes resulting from normal hair follicle physiology and specific gene alterations. However, to realize the true potential of MPM *in situ* optical tomography, a detailed evaluation of the relationship between observed signals and structure and/or function of the hair follicles and other systems under investigation still must be established in the near future.

2 Materials and Methods

The multiphoton laser scanning microscope used in this paper was described elsewhere.^{9,11} The laser excitation was linearly polarized at 760 or 800 nm. The two wavelengths were employed as part of the preliminary investigation for simultaneous optimal excitation of both intrinsic cellular fluorescence and SHG signals from the ECM within hair follicles. Spectral filtering with dichroic (500 nm) and bandpass filters were used to separate the SHG signal of the ECM in the internal structure of the hair follicle from that of intrinsic cellular fluorescence (380AF15 for $\lambda_{ex}=760$ nm and 400AF10 for $\lambda_{ex}=800$ nm). The cellular autofluorescence was further separated into blue (using a 445 ± 25 -nm filter) and red (using a 580 ± 30 -nm filter) components. Binary data were converted to 16-bit TIFF images using IPLab software (Scanalytics, Inc.). Three-dimensional reconstructions of hair follicles with tissue surrounding them and all corresponding sections were obtained using VoxBlast software (VayTek, Inc.).

All animal procedures were performed in accordance with an animal protocol approved by the University of California at Irvine. Mice strain CB6F1 was used in all experiments. Clim transgenic mice were generated by microinjection of the suitable plasmid into fertilized eggs implanted into healthy CB6F1 animals. These mice expressed the transgene in the basal cell layer of the epidermis, the outer root sheath of hair follicles, the basal cell layer of neonatal corneal epithelium, and limbal cells of adult corneal epithelium (Xu, unpublished). The transgenic mice exhibited corneal and skin abnormalities in addition to pathological hair cycling and differentiation. Immediately after euthanasia by asphyxiation with CO₂, the animals were shaved and subjected to 4 min treatment with Nair (Ralphs) to remove residual hair. The skins were surgically removed from the backs of the animals, cut into smaller pieces, and treated with dispase for two hours at 37°C to remove the epidermis. After the skins were rinsed with 0.9% saline solution, they were imaged with an inverted two-photon microscope. High-resolution 3-D reconstructions

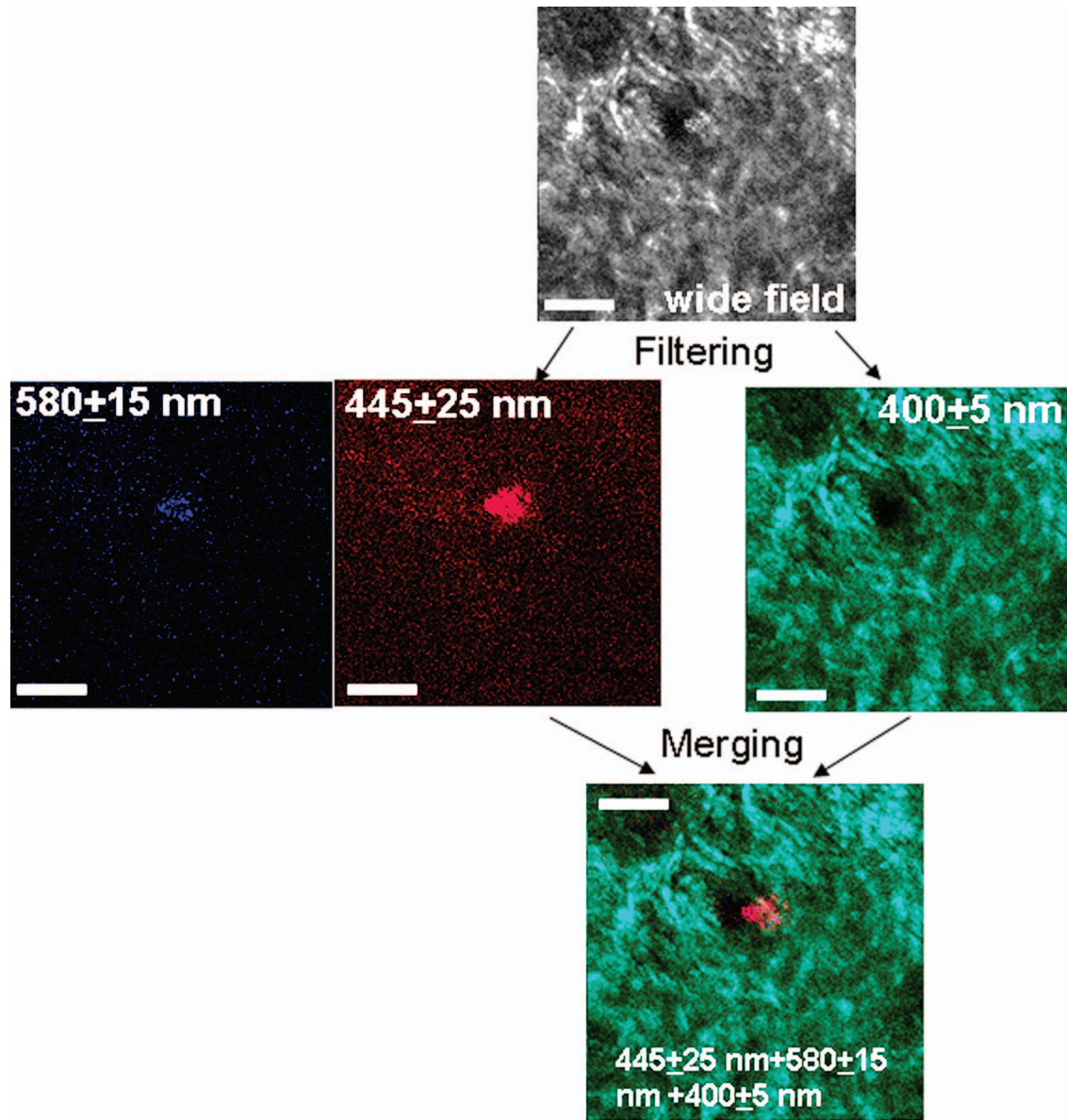


Fig. 2 Spectral filtering of MPM signals from a normal hair follicle. Images were obtained using the filters shown. Scale bar is 50 μm .

of the ECM and cellular structures up to 100 μm into the hair follicles were collected in under 5 min utilizing native signals only. The ages of the mice imaged were 5 months to about one year.

3 Results

To determine the capability of 3-D MPM tomography to map structural and functional properties of hair follicles *in situ*, we acquired multiple 3-D stacks of SHG and TPF coregistered images with the laser ($\lambda_{ex}=760/800\text{ nm}$) focused into the areas of the dermis containing hair follicles. Spectral filtering was used to effectively separate the SHG signals of the ECM in the hair follicle and native cellular fluorescence (Fig. 2). While most of the SHG signal is expected to be generated by the collagen of the dermal ECM, the observed intrinsic cellular fluorescence could result from many endogenous fluorophores distributed among the cells that comprise the complex

cellular architecture of the hair follicles. These fluorophores include keratins and melanin in addition to nicotinamide adenine dinucleotide (NADH) and oxidized flavin adenine dinucleotide (FAD). All these fluorophores can be simultaneously excited at a single near-infrared wavelength with low levels of photo-bleaching and without complications from inner-filter effects and light scattering previously unattainable with one-photon excitation. Once accurately quantified, SHG and TPF signals have the potential to be used to monitor tissue and cellular structural and functional dynamics and to serve as add-ons to many biochemical analyses.

Initially, to outline the overall structural organization of a typical hair follicle and the ECM that surrounds it in a normal mouse, we collected 3-D stacks at low magnification [Fig. 3(a)]. The transverse [Fig. 3(b)] and *en face* [Fig. 3(c)] optical sections are rapidly obtained from these 3-D stacks using commercial Voxblast software. The corresponding transverse

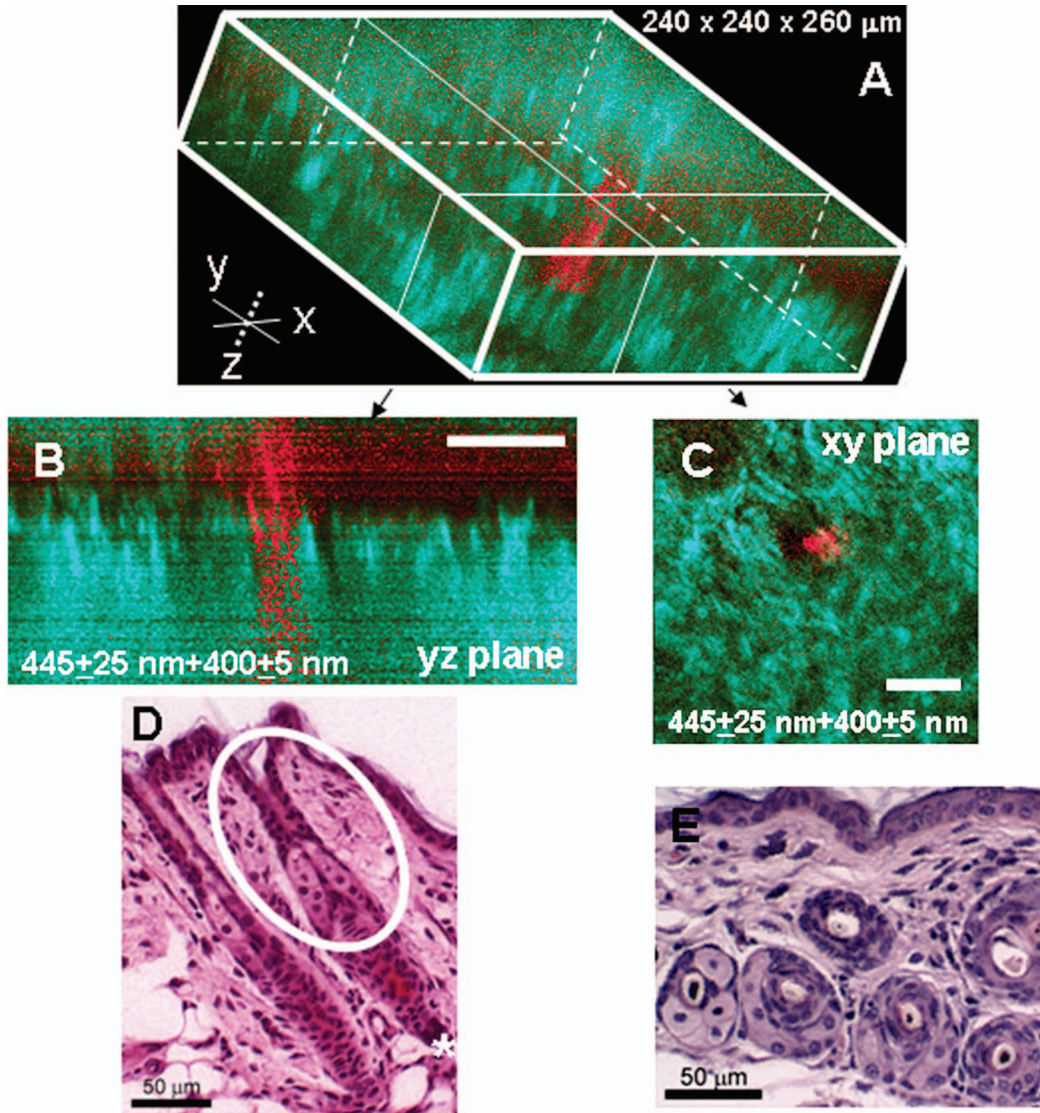


Fig. 3 (a) 3-D reconstruction of the normal hair follicle from the stack of MPM images taken at $2\text{-}\mu\text{m}$ increments. (b) Transverse optical section (yz plane) through a stack in (a). Scale bar is $50\ \mu\text{m}$. (c) *En face* optical section at $\sim 56\ \mu\text{m}$ through a 3-D stack in (a). Green: second harmonic signals (SHG) generated by ECM. Red: cellular fluorescence (TPF) detected with $445\pm 25\ \text{nm}$ filter. Scale bar is $50\ \mu\text{m}$. (d) A typical transverse histological section through the normal mouse telogen hair follicle with dermal papilla denoted by a star (\star). The oval outlines an approximate area visualized during MPM imaging. (e) A typical *en face* histological section of the hair follicles.

[Fig. 3(d)] and *en face* [Fig. 3(e)] typical histological sections of the normal hair follicles in mice at the same magnification are presented for comparison.

To better understand the structural features of the connective tissue surrounding the hair follicle [Fig. 4(a)] and hair-follicle-associated cellular components [Fig. 4(b)], we examined them independent of each other. The transverse yz section of the connective tissue [Fig. 4(a)] is rotated slightly relative to the complete reconstruction of a part of the dermis bearing a hair follicle in Fig. 3(a). It clearly outlines a portion of the ECM associated with a hair follicle that does not generate an SHG signal. It emerges as a gap in the ECM that starts at $\sim 28\ \mu\text{m}$ deep into the tissue and is especially pronounced on one side of the hair follicle (denoted by a star). We observed this space in all the hair follicles studied. At this time, we are not certain regarding its origin. It could indeed

be an empty space, in which case, we could speculate that it is usually utilized to house additional hair-follicle-associated cellular components removed during treatment with dispase. Alternatively, it could be filled with the dermal ground substance that is a major macromolecular component of connective tissue and is comprised of a broad class of anionic polysaccharides. These compounds are not expected to generate SHG or appreciable TPF signal upon infrared excitation. To illustrate cellular components of varying morphologies, we obtained serial xz transverse sections at different depths with Voxblast software [Fig. 4(b)].

To test the limits of MPM *in situ* optical tomography in resolving individual structural components of the hair follicle presented in Fig. 3, high-magnification *en face* MPM optical sections (Fig. 5) were collected. An optical section at $14\ \mu\text{m}$ inside the hair follicular structure exposes intricately shaped

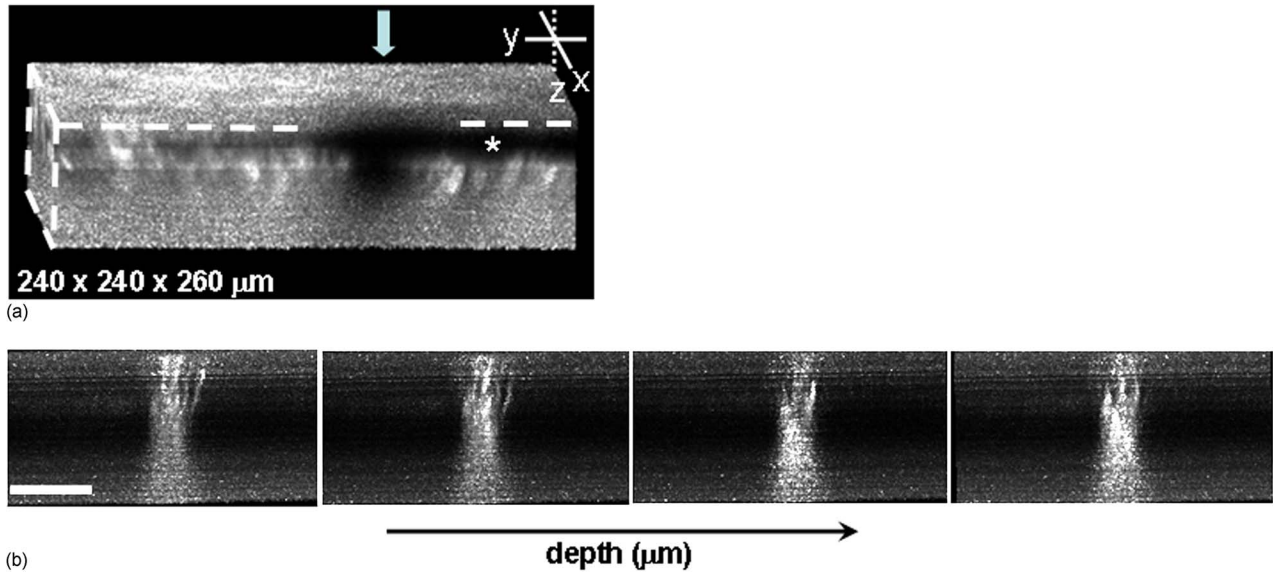


Fig. 4 (a) A transverse yz section through a 3-D reconstruction of the ECM in the normal hair follicle in Fig. 3(a) obtained from the stack of SHG images (400 ± 5 nm) taken at $2\text{-}\mu\text{m}$ increments. * denotes a gap (here it begins at about $28\ \mu\text{m}$) in the portion of ECM associated with hair follicle that does not generate an SHG signal. (b) Serial transverse optical xz sections through the cellular components of the hair follicle at $80\ \mu\text{m}$, $84\ \mu\text{m}$, $89\ \mu\text{m}$, and $93\ \mu\text{m}$. Scale bar is $50\ \mu\text{m}$.

cellular components packed against finger-like protrusions of the ECM filled with a material that does not appear to form fibrils resolvable by optical imaging in a backscattered configuration. In our MPM *in situ* optical tomography studies of normal mice dermis (unpublished data), the sizes of collagen bundles were greatest ($\sim 9\ \mu\text{m}$) throughout the thickness of reticular dermis. However, based on previous reports,²² the thickness of collagen bundles diminishes significantly in the fine connective tissue sheaths surrounding appendage structures (hair follicles), vessels, nerves, and papillary dermis where tissue volume consists of a greater percentage of the ground substance. Some cellular structures appear to be directly under and in contact with these flaps of the ECM. The axis of cellular orientation with an opening in the ECM is outlined with the dashed straight line, while the orifice of the hair follicle is denoted by an oval drawn over the image of the ECM at $\sim 14\ \mu\text{m}$ deep into the hair follicle. Interestingly, this opening in the ECM that accommodates cellular structures as well as orientations of cellular components with respect to that opening both make a turn defined by a dihedral angle denoted as β upon imaging deeper into the hair follicle. At $\sim 60\ \mu\text{m}$ deep into the hair follicle, the cellular fluorescence is still very strong. At this depth, the SHG signal from the ECM is only slightly visible on the margins of the image. It is not resolved because at this depth we are in a layer in the ECM that does not generate any significant SHG or fluorescence signal. To our knowledge, this is a first report of imaging this deep into the hair follicle structures using native signals only with such high contrast and therefore opens a possibility to quantitatively and accurately estimate hair-follicle-associated geometric parameters *in situ*.

Figure 6(a) shows another hair follicle observed at high resolution during *in situ* multiphoton imaging. Structurally different cellular components compared to the follicle in Fig. 3 are noted. It is difficult to understand at this time the under-

lying origins of this difference due to the complex changes in cellular morphology and possibly structural and chemical composition of the ECM—both of which are associated with hair cycling. One explanation could be that the differentiation state of this hair follicle is different from the one in Fig. 3. The topmost images do not display cellular fluorescence because the outer layer of the hair follicle is contiguous with epidermis and was most likely removed by dispase. However, an optical section at $29\ \mu\text{m}$ inside the hair follicular structure exposes cells tightly packed against similar finger-like protrusions of the ECM observed for the follicle in Fig. 5. Similar to Fig. 5, these portions of the ECM appear to be composed from a material that does not form fibrils resolvable by optical imaging in a backscattered configuration. These types of high-resolution images could be utilized, for example, to determine angles of cellular components with respect to the surface of the connective tissue angle α ; [Fig. 6(b)].

For comparison, Fig. 6(c) shows a typical hematoxylin and eosin (H&E)-stained *en face* histology section through a hair follicle. The structural features of the surrounding connective tissue inside the hair follicle and its interaction with cellular components are completely gone in histologically processed tissues. The follicles artificially appear as rounded craters with shrunken cells inside them. In the highest quality histological sections, the perplexing involutions of the ECM apparent in the SHG images are reduced to a “wavelike” line structure due to the chemical processing of tissues required for histological analysis.

Preliminary examination of the hair follicles in a transgenic mouse model of a *Clim*^{15–20} transcriptional factor involved in organ development and cancer revealed modified interactions of the ECM with the cellular components. In the terminal phenotype of a *Clim* transgenic mouse, cellular fluorescence was absent from most hair follicles examined [Fig. 7(a)]. Since *Clim* transgenic mice express the transgene in the

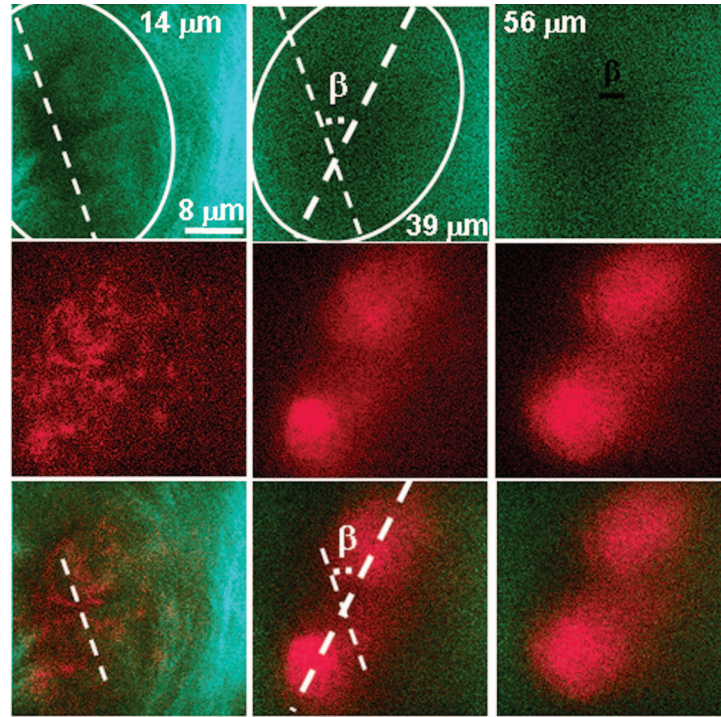


Fig. 5 *En face* high-resolution MPM optical sectioning of the normal hair follicle in Fig. 3. Color coding is the same as in Fig. 3. In addition to the angle α formed by hair-follicle-associated cells with the surface of the skin, a dihedral angle β associated with the twist of the opening in the connective tissue to accommodate the cellular structures is noted in the images.

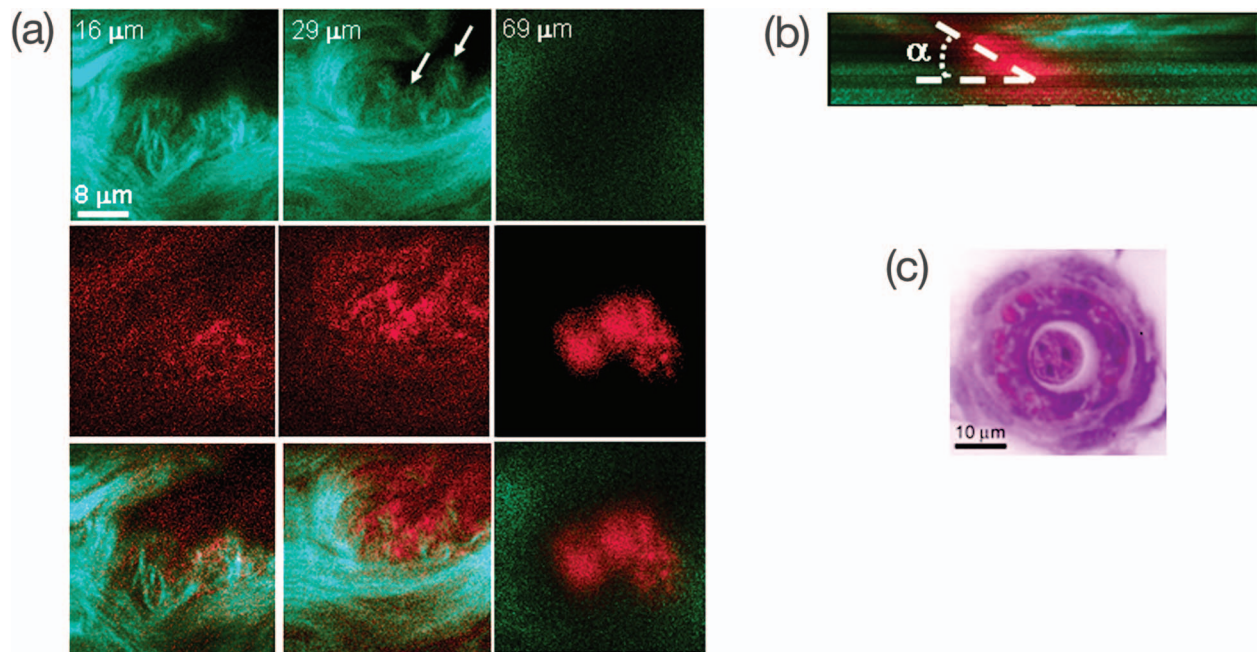


Fig. 6 (a) *En face* MPM optical sectioning of the normal hair follicle. Top: ECM; arrows denote involutions of ECM filled with material that does not appear to form fibrils resolvable by optical imaging in a backscattered configuration. Middle: cellular structures. Bottom: color images consisting of two species—ECM (green); cellular structures (red) packed against an opening in ECM. (b) Angle α of cellular components with respect to the surface of the connective tissue could be obtained from high-resolution 3-D reconstructions of hair follicles based on endogenous signals only. (c) High-resolution *en face* histological section through a normal mouse hair follicle. For all MPM images, SHG generated by ECM is green and cellular fluorescence (TPF) detected with a 445+25 nm filter is red.

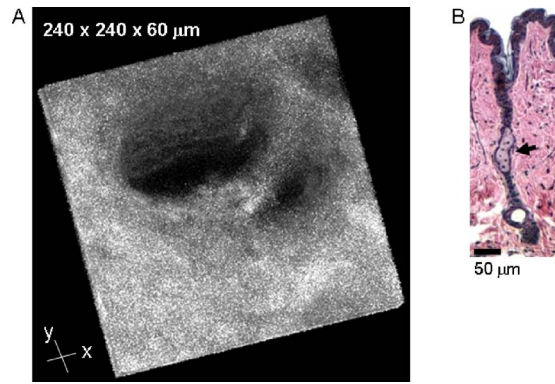


Fig. 7 (a) Low-resolution ($NA=0.3$) 3-D reconstruction of the terminal phenotypic pathological hair follicle. Second harmonic signal only; cellular structures were absent in the majority of hair follicles studied. (b) A typical transverse histological section through a terminal phenotypic pathological hair follicle. A change in the sebaceous gland is denoted by an arrow.

basal layer of the epidermis (and outer root sheath of the hair follicles), it is plausible to assume that alteration of the *Clim* transcriptional factor resulted in modified basement membrane adhesion proteins (for example, collagen VI and/or collagen VII), therefore compromising the connectivity of cellular structures to the dermis. It is also possible that they were more susceptible to digestion with dispase and were subsequently removed more easily during tissue handling compared to the normal phenotype. The angles of the follicular orifices in these pathological hair follicles were very shallow compared to those in the normal mice. Such modification in the overall internal 3-D geometries of the opening in the ECM in the transgenic hair follicles could occur as a result of changes in the cellular structures, for example, a sebaceous gland [Fig. 7(b)].

4 Discussion and Conclusions

In this report, we demonstrate that MPM imaging combining backscattered SHG and two-photon fluorescence signals offers a powerful approach to map the structural and functional organization of hair follicles during their normal and altered physiology (development) *in situ* rapidly with high resolution and contrast. The sizes of follicular orifices, angles of cellular components with respect to the surface of the connective tissue, and overall 3-D geometries including rotations of the openings in the ECM (described in this paper by dihedral angles) that accommodate cellular components can be quantitatively studied. While much more work needs to be done to evaluate the significance of this later feature, it is relevant to postulate that it had possibly evolved as a mechanism to establish appropriate electrostatic and steric interactions of the ECM with cellular structures inside the hair follicles. Since the angle of the hair shaft and hair-follicle-associated cells is genetically controlled, a possible assumption would be that this angle as well as the dihedral angle will be sensitive to a physiological state of the hair follicle. Therefore, we are creating structural and functional follicular maps of the ECM and hair-follicle-associated cells during specific points of the hair cycle²³ in mice and correlating those with the gene and protein expression profiles. This biologically controlled study

will bring multiphoton optical tomography closer to being relevant to *in vivo* clinical and basic medical research of hair. The growing wealth of data suggests that follicular drug absorption plays an important role in drug delivery mechanisms for the topically applied drugs. Therefore, a quantitative methodology based on multiphoton imaging could be established to optimize follicular drug delivery and to study complex mechanisms of drug effects on ECM and remodeling of the hair follicle associated cells *in situ*. Additionally, rapid technological improvements in fiber-optic scanning two-photon endoscopy²⁴ will potentially move minimally invasive optical histologic imaging of skin forward and offer significant contributions to *in vivo* clinical and basic medical research of hair in the near future.

Diffraction-limited resolution of MPM imaging is comparable to that of histology; however, the absence of chemical tissue processing and staining reduces the number of artifacts introduced into the samples prepared for and analyzed by histology or electron microscopy. Therefore, we see *in situ* multiphoton optical tomography to be especially valuable in examining genetically altered hair follicles and various connective tissues. These tissues often display aberrant mechanical responses due to disturbed overall organization, content, and physical properties of collagen fibers,²⁵ therefore making it cumbersome to rely on histology as a means of correlating the genetically induced structural pathologies with gene and protein expression profiles.

A common mechanism has been suggested for the downward growth of the early anagen hair follicle and invading basal or squamous carcinomas.²⁶ For the cells to penetrate the dermis during the early anagen phase, the follicles have been shown to lyse collagen gels *in vitro* and to synthesize various matrix metalloproteinases (MMPs) including collagenase *in vivo*.²⁶ Ultimately, the nondestructive quantitative imaging studies of normal and pathological hair follicles coupled with better understanding of the complex molecular mechanisms involved in hair cycling will lead to improved insights regarding the difference between controlled degradation of ECM observed during a coordinated process of constant remodeling of normal hair follicle as compared to disruptions observed in skin cancers.

Acknowledgments

Julia G. Lyubovitsky thanks George E. Hewitt and George E. Hewitt Foundation for Medical Research for a three-year postdoctoral fellowship. We greatly thank Ki Hean Kim, Daekeun Kim, and Peter So for help with software and hardware development of our two-photon microscope. This study was made possible, in part, through the NIH Laser Microbeam and Medical Program (LAMMP) at the University of California, Irvine, (P41-RR01192) and by the Air Force Office of Scientific Research (AFOSR), under Agreement No. FA9550-04-1-0101. Bogi Andersen is supported by NIH Grant NO. AR44882.

References

1. E. Brown, T. McKee, E. DiTomaso, A. Pluen, B. Seed, and Y. Boucher, *Nat. Med.* **9**, 796–801 (2003).
2. P. J. Campagnola, H. A. Clark, W. A. Mohler, A. Lewis, and L. M. Loew, *J. Biomed. Opt.* **6**, 277–286 (2001).

3. P. J. Campagnola, A. C. Millard, M. Terasaki, P. E. Hoppe, C. J. Malone, and W. A. Mohler, *Biophys. J.* **82**, 493–508. (2002).
4. P. J. Campagnola, M. D. Wei, A. Lewis, and L. M. Loew, *Biophys. J.* **77**, 3341–3349 (1999).
5. R. Gauderon, P. B. Lukins, and S. J. Sheppard, *Micron* **32**, 691–700 (2001).
6. Y. Guo, H. E. Savage, F. Liu, S. P. Schantz, P. P. Ho, and R. R. Alfano, *Proc. Natl. Acad. Sci. U.S.A.* **96**, 10854–10856 (1999).
7. L. Moreaux, O. Sandre, M. Blanchard-Desce, and J. Mertz, *Opt. Lett.* **25**, 320–322 (2000).
8. L. Moreaux, O. Sandre, S. Charpack, M. Blanchard-Desce, and J. Mertz, *Biophys. J.* **80**, 1568–1574 (2001).
9. A. Zoumi, A. Yeh, and B. J. Tromberg, *Proc. Natl. Acad. Sci. U.S.A.* **99**, 11014–11019 (2002).
10. A. T. Yeh, N. Nassif, A. Zoumi, and B. J. Tromberg, *Opt. Lett.* **27**, 2082–2084 (2002).
11. J. G. Lyubovitsky, T. B. Krasieva, J. A. Spencer, B. Andersen, and B. J. Tromberg, *J. Biomed. Opt.* **11**, 014013 (2005).
12. K. S. Stenn, *Physiol. Rev.* **81**, 449–488 (2001).
13. Shi C., Y. Zhu, Y. Su, and T. Cheng, *Biotechnology* **24**, 48–52 (2006).
14. H. B. Chase, *Physiol. Rev.* **34**, 113–126 (1954).
15. A. D. Agulnick, M. Taira, J. J. Breen, T. Tanaka, I. B. Dawid, and H. Westphal, *Nature (London)* **384**, 270–272 (1996).
16. I. Bach, C. Carriere, H. P. Ostendorff, B. Andersen, and M. G. Rosenfeld, *Genes Dev.* **11**, 1370–1380 (1997).
17. L. W. Jurata, D. A. Kenny, and G. N. Gill, *Proc. Natl. Acad. Sci. U.S.A.* **93**, 11693–11698 (1996).
18. T. M. Sugihara, I. Bach, C. Kiousi, M. G. Rosenfeld, and B. Andersen, *Proc. Natl. Acad. Sci. U.S.A.* **95**, 15418–15423 (1998).
19. E. Torigoi, I. M. Bennani-Baiti, C. Rosen, K. Gonzalez, P. Morcillo, M. Ptashne, and D. Dorsett, *Proc. Natl. Acad. Sci. U.S.A.* **97**, 2686–2691 (2000).
20. J. E. Visvader, X. Mao, Y. Fujiwara, K. Hahm, and S. H. Orkin, *Proc. Natl. Acad. Sci. U.S.A.* **94**, 13707–13712 (1997).
21. X. Xu, J. A. Spencer, K. K. Lin, E. I. Kudryavtseva, and B. Andersen.
22. L. A. Goldsmith, Oxford University Press, New York, 1991, pp. 869.
23. K. K. Lin, D. Chudova, G. W. Hatfield, P. Smyth, and B. Andersen, *Proc. Natl. Acad. Sci. U.S.A.* **101**, 15955–15960 (2004).
24. M. T. Myaing, D. J. MacDonald, and X. Li, *Opt. Lett.* **31**, 1076–1078 (2006).
25. K. G. Danielson, H. Beribault, D. F. Holmes, H. Graham, K. E. Kadler, and R. V. Iozzo, *J. Cell Biol.* **136**, 729–743 (1997).
26. V. M. Kahari and U. K. Saarialho-Kere, *Exp. Dermatol.* **6**, 199–213 (1997).